ATMOSPHERIC DYNAMICS

Hydraulic jump dynamics above supercell thunderstorms

Morgan E O'Neill[1]*, Leigh Orf[2,3], Gerald M. Heymsfield[4], Kelton Halbert[2]

The strongest supercell thunderstorms typically feature an above-anvil cirrus plume (AACP), which is a plume of ice and water vapor in the lower stratosphere that occurs downwind of the ambient stratospheric flow in the lee of overshooting deep convection. AACP-origin hydration of the stratosphere has a poorly constrained role in ozone destruction and surface warming. In this study, we use large eddy simulations corroborated by radar observations to understand the physics of AACP generation. We show that the overshooting top of a simulated supercell can act as a topographic obstacle and drive a hydraulic jump downstream at the tropopause, similar to a windstorm moving down the slope of a mountain but without solid topography. Once the jump is established, water vapor injection deep into the stratosphere may exceed 7 tonnes per second.

Above-anvil cirrus plumes (AACPs) are a regular feature of strong mid-latitude thunderstorms, particularly over the Great Plains (*1*–*4*). AACPs exhibit a high correspondence with the most severe conditions on the ground, including major tornado and hail events (*4*–*6*). An AACP consists of a thin cirrus plume, often visible by satellite, which shoots several kilometers above the much larger anvil cloud directly into the lower stratosphere where it spreads downwind. AACPs can also aid in the predictability of severe hail and tornadoes, as AACPs are visible above the cloud tops an average of 31 min before severe conditions are reported (*6*).

AACPs may also play a major role in water vapor injection into the lower stratosphere (*2*, *5*, *7*), which is hydrated by deep convection (*8*, *9*). Increased stratospheric water vapor increases stratospheric radiative cooling directly and through ozone destruction (*10*–*12*) but acts to warm the troposphere and surface (*13*, *14*). Model-based estimates of the water injection rate into the lower stratosphere above a deep thunderstorm range from 1 to a few tonnes of water per second on average (*2*, *15*–*18*), suggesting deep convective origin of total stratospheric water vapor, as high as 18% from tropical storms alone (*18*). Thunderstorm frequency may increase owing to a rise in atmospheric specific humidity in a warming climate (*19*), which suggests the potential for positive feedback between more mid-latitude thunderstorms and increased lower stratospheric water vapor in response to climate change (*20*).

AACP dynamics and associated features, particularly the physical mechanism responsible for irreversibly injecting tropospheric water into the lower stratosphere, are an issue of debate, though there is broad agreement regarding the role of breaking gravity waves excited by deep convection (*1*, *2*, *4*, *5*, *21*). It has long been recognized that deep convection and overshooting tops (OTs) can effectively act as topography that can block or redirect oncoming upper tropospheric or stratospheric air (*1*, *21*). This can lead to the breaking of waves downstream, which lofts water into the lower stratosphere (*2*). However, there are a half dozen concurrently observed features for which there is still no consistent physical model, and existing hypotheses appear to contradict each other. We resolve these conflicts by showing that the mechanism responsible is likely a hydraulic jump, forced by and interacting with the dynamic OT. Hydraulic jumps occur when fluid flows too fast for gravity waves to travel upstream, wherein the fluid becomes unstable and suddenly readjusts to a turbulent, slower flow.

Homeyer *et al.* (*5*) were the first to identify the mean environmental conditions that determine whether an AACP forms. They identified the importance of upper-level wind magnitude and, through idealized numerical simulations, showed that stronger constant oncoming winds in the upper troposphere and lower stratosphere induce a strong AACP, whereas winds of half that magnitude do not.

In this study, we conducted two large eddy simulation (LES) experiments using modifications to the Homeyer *et al.* (*5*) soundings (fig. S1): one with strong upper winds, simU_{str}, and one with weak upper winds, simU_{wk} (*22*). These idealized wind profiles are based on reanalysis results (*5*). The Bryan Cloud Model 1 (*23*) is run at 50-m cubic resolution in a storm-following domain of size 243.2 km by 240.8 km by 30 km. We find that most of the competing AACP hypotheses can be simultaneously correct, each explaining a different aspect of a downslope windstorm and hydraulic jump at the tropopause. Regarding the simU_{wk} storm, we provide an observation of a similar storm observed in May 2011 that likely exhibits an example of flow separation above the OT, which precludes a hydraulic jump. Finally, we quantify how much water is irreversibly injected into the lower stratosphere by each simulated storm.

Both simulations rapidly develop a mature supercell thunderstorm with a cold OT that reaches a height of ~15 km, generating gravity waves in its environment (Fig. 1 and figs. S2 and S3). The storm-relative upper winds are 33.7 m s^{-1} for simU_{str} and 14.5 m s^{-1} for simU_{wk}. Storm simU_{str} eventually develops a steady AACP, and simU_{wk} does not.

The upper flow behavior of simU_{str} and simU_{wk} differs noticeably by minute 35, approximately when the OT in each storm becomes established well above the 12-km tropopause (fig. S3). simU_{wk} exhibits flow separation of stratospheric air away from the storm anvil shortly after cresting the OT, similar to flow separation in the lee of real topography. This separation prevents the development of a strong standing gravity wave, and the free-slip–like conditions instead permit weak transient overturning circulations (rotors) (*24*). By contrast, simU_{str} exhibits a deepening standing gravity wave in the lee of the OT.

Before the OT altitude becomes relatively steady, the simU_{str} storm develops a turbulent filament of breaking gravity waves aloft, in a narrow region 2 to 3 km above and ~5 km downstream of the simU_{str} OT (*25*). It is narrowly rooted in the cloud top but spreads out forward and laterally such that it lies above nearly laminar flow (Fig. 1A and fig. S4). By minute 40, this turbulent region is identified by turbulent kinetic energy dissipation values >5 m^2 s^{-2}, indicating substantial mixing. Concurrently, the simU_{str} storm develops a broad, rapid jet exceeding speeds of 75 m s^{-1} at the tropopause. By minute 45, simU_{str} exhibits the onset of a hydraulic jump and a type II rotor (Fig. 1C) (*26*). Meanwhile, the flow separation in the lee of the simU_{wk} storm's OT allows the development and formation of a milder type I rotor between the tropospheric jet below and smooth stratospheric flow above (Fig. 1 and fig. S3).

Lagrangian parcel analysis of simU_{str} reveals that the fastest wind region at the tropopause (speed >110 m s^{-1}) is sourced primarily from the core of the overshooting updraft but also from the lower stratosphere (Fig. 2), a mixing hypothesized by Heymsfield *et al.* (*21*). Most upstream stratospheric air in simU_{str} below the peak altitude of the OT diverges around it. However, some stratospheric air above the OT's central axis plunges downward from 17- to 12.5-km altitude in the lee

[1]Department of Earth System Science, Stanford University, Stanford, CA 94305, USA. [2]Space Science and Engineering Center, University of Wisconsin, Madison, WI, USA. [3]Cooperative Institute for Meteorological Satellite Studies, Madison, WI, USA. [4]NASA Goddard Space Flight Center, Greenbelt, MD, USA.
*Corresponding author. Email: morgan.e.oneill@gmail.com

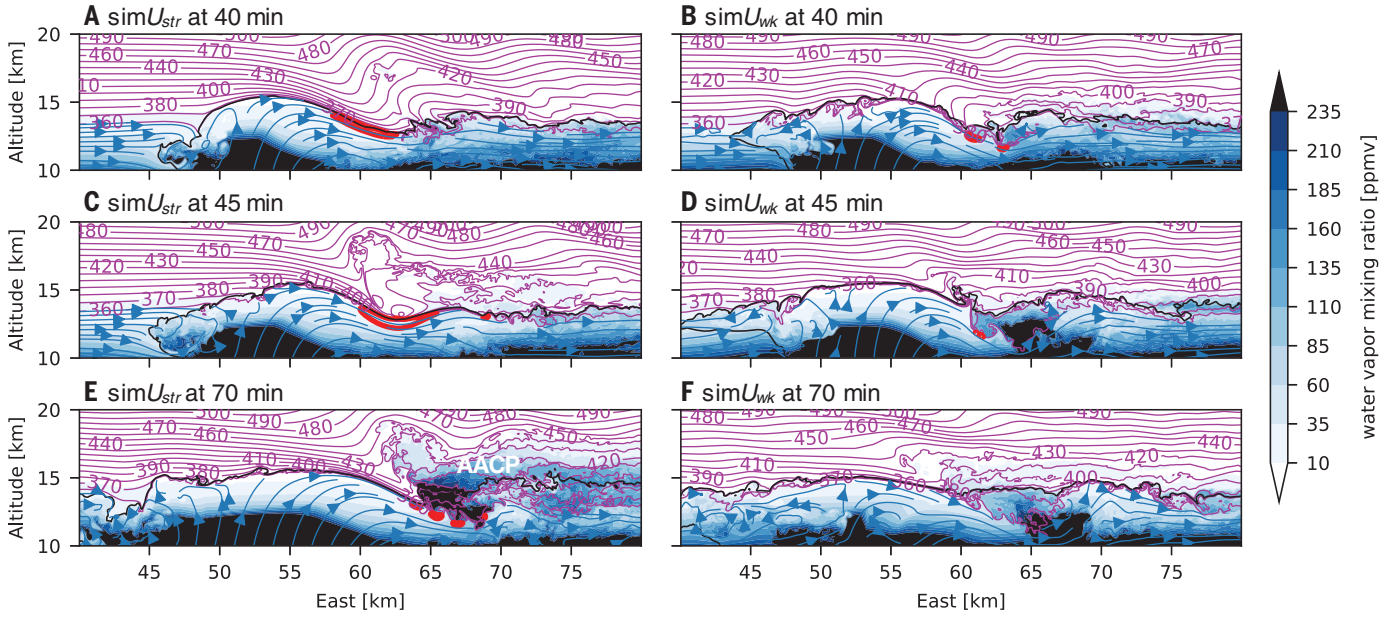

Fig. 1. Storm evolution. Cross-section of simU_{str} (**A**, **C**, and **E**) and simU_{wk} (**B**, **D**, and **F**) at *y* locations indicated in fig. S2. Magenta lines, potential temperature above 360 K; blue lines, streamlines below 360 K; red contour, region where total wind speed >75 m s^{-1}; blue shading, water vapor mixing ratio in parts per million by volume (ppmv); black line, cloud and frozen water mass mixing ratio of 5 × 10^{-2} g kg^{-1}. The general location of the AACP is labeled in (E).

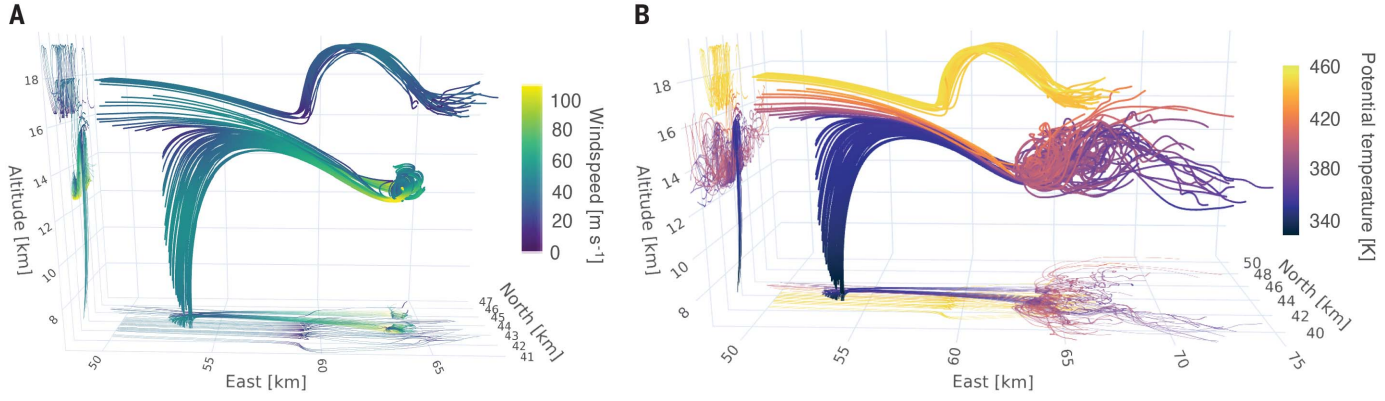

Fig. 2. Lagrangian parcels that meet one of the following conditions: Total wind speed exceeds 110 m s^{-1} within the jet before entering the hydraulic jump ("jump parcels"), or maximum height exceeds 19.25 km ("lid parcels"). (**A**) Parcels are shaded by wind speed, lid parcels are integrated from 40 to 50 min, and jump parcels are integrated from 40 to 46 min to visualize the breaking wave. (**B**) Same parcels are shaded by potential temperature; jump parcels are integrated from 40 to 51.7 min to visualize mixing. For text and interactive 3D versions, see supplementary materials.

of the OT. Negatively buoyant, descending tropospheric air from the OT converges in the same jet, and a tropospheric parcel reaches a storm-relative peak speed of 119 m s^{-1}.

The simU_{str} OT is exceedingly cold, with the coldest parcels nearing 190 K. Frozen water in the moist tropospheric updraft precipitates out (graupel) or descends in the subsiding jet region (ice), and tropospheric air is diabatically warmed as a result of mixing (Fig. 2B). The potential temperature of tropospheric parcels exceeding 90 m s^{-1} increases in the range of 0 to 100 K in total, with most of the increase occurring rapidly once the now-dehydrated air enters the turbulent jump (fig. S5). Jet-bound stratospheric air plummets down the leeside of the OT, where it is adiabatically warmed by more than 25 K within 15 km downstream of the OT (fig. S6), consistent with (*27*) though over half the distance. It is also substantially hydrated through mixing with tropospheric air.

Using airborne radar, we observed a feature that bears similarity to breaking waves in the OT lee of both simulations (though primarily simU_{wk}), lending credence to the realism of our simulations. The NASA ER-2 aircraft flew over an intense, nontornadic hailstorm in Oklahoma on 24 May 2011 (Fig. 3, A, C, and E, and fig. S7) during the Mid-latitude Continental Convective Clouds Experiment (MC3E) (*28*, *29*). The aircraft was instrumented with a dual-frequency nadir-pointing Doppler radar. One of the storms, which had an extremely strong updraft estimated at 50 m s^{-1} and an OT at 16-km altitude (tropopause height ~14 km), also had an apparent Kelvin-Helmholtz (K-H) wave on the lee side of the OT. Rising and sinking motions from the Doppler velocities (Fig. 3E) are consistent with the presence of a K-H wave.

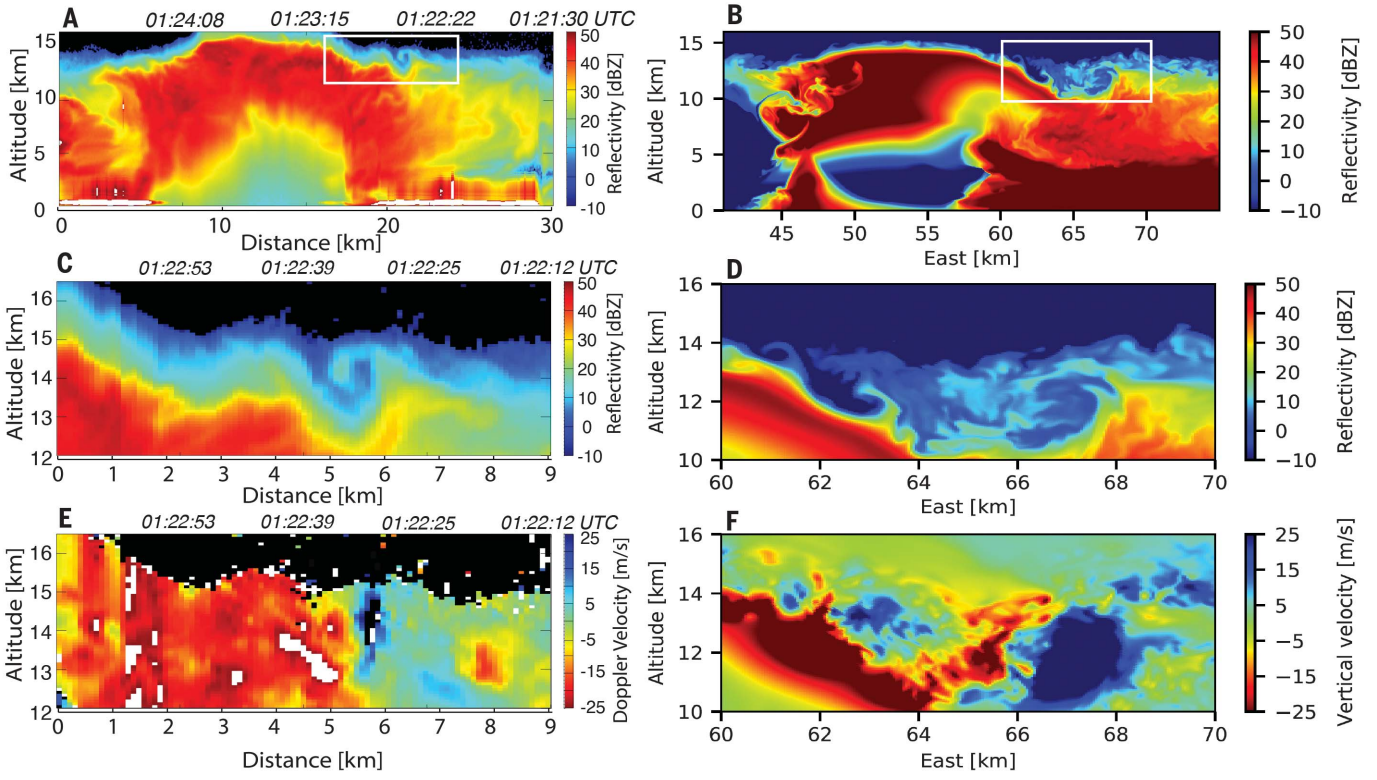

Fig. 3. Comparison of K-H wave at storm top observed by ER-2 HIWRAP Radar during storm transect on 24 May 2011 at 0125 UTC (Universal Time Coordinated) and simulation simU_{wk}. In both cases the stratospheric wind blows from left to right. (**A**) Doppler Ku-band radar reflectivity of the entire transect. (**B**) Simulated reflectivity of simU_{wk}, minute 55 in *xz* cross section at y = 34.925 km. (**C**) Doppler Ku-band radar reflectivity of K-H wave; (**D**) same as (C) but for simU_{wk} candidate K-H feature. (**E**) Doppler estimated vertical velocity (saturated at ±25 m s^{-1}) of K-H wave in (C). (**F**) Simulated vertical velocity of K-H wave in (D) (color bar saturated at ±25 m s^{-1}).

Similar transient K-H features are found in simU_{wk}, and we show a candidate in Fig. 3, B, D, and F. The storm-relative environmental wind speed at 14 km is ~14 m s^{-1} (fig. S8), similar to simU_{wk}'s wind speed of 14.5 m s^{-1}, though the observed storm also had wind shear in that region. The corresponding flow field in simU_{wk} demonstrates that in the lee of the OT, a layer of stratospheric air is stagnant above a region of faster tropospheric air (fig. S9). This permits K-H wave breaking of the descending tropospheric air from the OT to occur in the absence of a hydraulic jump, as well as formation of a weak type I rotor just above it.

The impact of the AACP on local stratospheric hydration is substantial. Simulated water injection into the stratospheric middleworld (between 360 and 380 K potential temperature surfaces) and overworld (above 380 K) is measured by a time series of the domain-integrated perturbation water vapor and frozen water for both storms (Fig. 4, A and B). In the unsaturated stratosphere, sublimation of ice is an irreversible process, so the water vapor time series integrates the contribution of both direct injection and sublimation of injected ice. Overall, simU_{wk} is a broader storm and a better hydrator of the stratosphere. By the end of the simulation, simU_{wk} has injected slightly more water vapor than simU_{str} into the middleworld and ~50% more ice. However, the bulk of this water vapor reaches only the thin lower layer of the stratospheric middleworld.

Though both storms induce gravity wave breaking at the tropopause early on, there is a substantial divergence of overworld water injection at $t \approx 45$ min in simU_{str}, coincident with the occurrence of the peak wind in the jet region and the jump onset (Fig. 4). Upon reaching the jump onset, the stratospheric overworld in simU_{str} experiences an increase in water vapor mass at a rate of ~7.6 tonnes s^{-1}, which is the highest yet quantified in a simulation. By contrast, simU_{wk} exhibits an overworld vapor injection rate of ~1.3 tonnes s^{-1}, which is itself unexpectedly high.

The linear trends of water injection indicate that both storms had much future potential to inject water into the stratosphere. Greatly heightened stratospheric water vapor mixing ratios have been observed downstream of deep mid-latitude convection up to a day later (*9*), suggesting that this short model integration is irreversibly injecting water into the stratosphere.

The severe storm community has long considered OTs to be "topographic" obstacles, inducing lee waves and potentially rotors. This work suggests the presence of hydraulic control, supercritical flow, and a hydraulic jump in the lee of a thunderstorm's OT, at the tropopause. Similar behavior has been observed and modeled for decades by the mountain meteorology community. Theoretical work motivated by severe downslope windstorms in the lee of mountains (*30*–*33*) may be applicable to the prediction of severe thunderstorm behavior.

Internal hydraulic theory has been developed for continuously stratified flow above real topography (*30*, *33*). There are three mechanisms by which a continuous, unbounded atmosphere above an obstacle may initiate a downslope windstorm that terminates in a hydraulic jump (*34*). All three require a vertical length scale that serves the place of an upper boundary from classic hydraulic theory, and this is commonly provided by either vertical shear or a change in the environmental buoyancy frequency with height. Because the ratio of the buoyancy frequency (N) to the mean wind speed (U) is approximately constant with height in the stratosphere of the present simulations, the only capping mechanism available is that sufficient gravity wave breaking occurs aloft of a topographic obstacle and

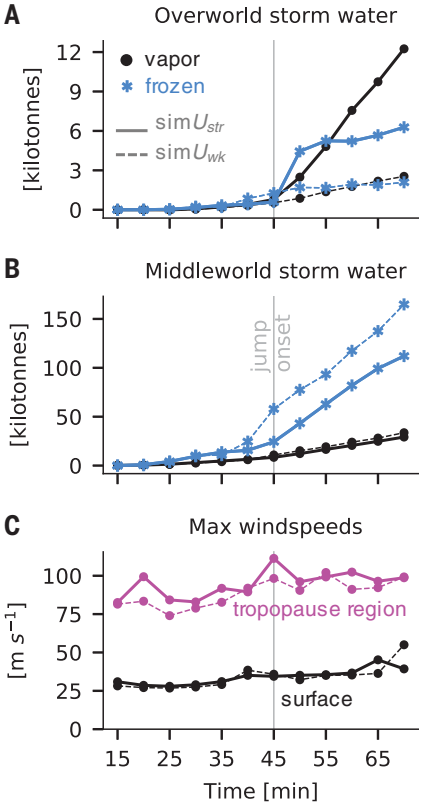

Fig. 4. Temporal evolution of water mass and wind in simU_{str} and simU_{wk} in kilotonnes. Mass unit is 1 tonne = 1000 kg. (**A**) Perturbation water content (black circles for vapor and blue snowflakes for solid phases) in the model domain in the stratospheric overworld above the 380 K potential temperature surface for simU_{str} (solid line) and simU_{wk} (dashed line). (**B**) Similar to (A) except in the stratospheric middleworld 360 to 380 K layer. (**C**) Peak wind speed in the storm vicinity in the tropopause region (magenta, 11- to 14-km altitude) and near the surface (black, 25 m altitude). Jump onset in simU_{str} is indicated by the gray vertical line in each panel.

forms a wave-induced critical layer at that height. This layer can then serve to trap and reflect vertically propagating gravity waves back downward and eventually lead to the development of a hydraulic jump in continuously stratified flow (*35*).

One might measure a nondimensional obstacle height $\hat{h}_m = Nh_m/U$ to understand lee flow behavior as a function of incoming horizontal wind speed U, buoyancy frequency N, and topographic height h_m (*4*). Though the OT reaches 15 km, 3 km above the base state tropopause, stratospheric air that is lifted and advected over the OT rises no more than 200 m ($h_m \approx 200$ m). Most air is deflected around the storm laterally. Though this yields $\hat{h}_m < 1$ for simU_{str}, $\hat{h}_m$ is not the only control that determines wave breaking aloft or downstream, and a hydraulic jump can still occur when $\hat{h}_m < 1$ (*31*).

The primary departure from the downslope windstorm mechanism is the finding that air exiting the OT speeds up into the jet region as it subsides downwind in both simulations, apparently independent of whether the stratosphere converges into it or separates aloft. The jet can exceed speeds of 90 m s^{-1} even in simU_{wk} (Fig. 4C). This feature has no counterpart in real topographic obstacles because it is the topography itself that is flowing, and h_m varies with the evolving OT shape. A jet in the OT lee of both storms seems inevitable as the collapsing OT must accelerate downward in the lee toward its level of neutral buoyancy (*1*).

This work demonstrates a likely internal hydraulic jump in the absence of solid topography. More realistic wind profiles near and above the tropopause can have considerable shear, which can be a more favorable environment for the occurrence of a hydraulic jump (*34*). Though the presence of water species does not seem to have much effect on AACP dynamics, subsequent water injection to the stratosphere greatly increases stratospheric humidity during the duration of the simulation.

The realism of the rapid tropopause jet found in an AACP-producing storm can be validated using the existing high-altitude ER-2 airborne platform. Improvements in the radars aboard the ER-2 include scanning for 3D winds and higher sensitivity. Additionally, a cloud lidar that detects small ice particles often accompanies these radars. A dedicated field campaign that targets AACP-generating convective storms at close range would better constrain storm top physics and quantify their water vapor contribution to the stratosphere; this would be complementary to the ongoing NASA Dynamics and Chemistry of the Summer Stratosphere (DCOTSS) campaign taking place 2021–2022.

REFERENCES AND NOTES

1. T. T. Fujita, *J. Meteorol. Soc. Jpn. Ser. II* **60**, 355–368 (1982).
2. P. K. Wang, *J. Geophys. Res. Atmos.* **108**, 4194 (2003).
3. K. Bedka *et al.*, *J. Appl. Meteorol. Climatol.* **49**, 181–202 (2010).
4. C. R. Homeyer, *J. Atmos. Sci.* **71**, 332–348 (2014).
5. C. R. Homeyer, J. D. McAuliffe, K. M. Bedka, *J. Atmos. Sci.* **74**, 1617–1633 (2017).
6. K. Bedka, E. M. Murillo, C. R. Homeyer, B. Scarino, H. Mersiovsky, *Weather Forecast.* **33**, 1159–1181 (2018).
7. M. E. E. Hassim, T. P. Lane, *Atmos. Chem. Phys.* **10**, 9833–9849 (2010).
8. T. Corti *et al.*, *Geophys. Res. Lett.* **35**, 35 (2008).
9. J. B. Smith *et al.*, *J. Geophys. Res. Atmos.* **122**, 9529–9554 (2017).
10. D. T. Shindell, *Geophys. Res. Lett.* **28**, 1551–1554 (2001).
11. C. A. Smith, J. D. Haigh, R. Toumi, *Geophys. Res. Lett.* **28**, 179–182 (2001).
12. J. G. Anderson *et al.*, *Proc. Natl. Acad. Sci. U.S.A.* **114**, E4905–E4913 (2017).
13. P. M, *Geophys. Res. Lett.* **26**, 3309–3312 (1999).
14. S. Solomon *et al.*, *Science* **327**, 1219–1223 (2010).
15. J.-P. Chaboureau *et al.*, *Atmos. Chem. Phys.* **7**, 1731–1740 (2007).
16. C. Chemel, M. R. Russo, J. A. Pyle, R. S. Sokhi, C. Schiller, *Mon. Weather Rev.* **137**, 2493–2514 (2009).
17. X. M. Liu *et al.*, *Atmos. Chem. Phys.* **10**, 8267–8286 (2010).
18. T. Dauhut, J.-P. Chaboureau, J. Escobar, P. Mascart, *Atmos. Sci. Lett.* **16**, 135–140 (2015).
19. R. J. Trapp *et al.*, *Proc. Natl. Acad. Sci. U.S.A.* **104**, 19719–19723 (2007).
20. A. E. Dessler, M. R. Schoeberl, T. Wang, S. M. Davis, K. H. Rosenlof, *Proc. Natl. Acad. Sci. U.S.A.* **110**, 18087–18091 (2013).
21. G. M. Heymsfield, R. H. Blackmer, S. Schotz, *J. Atmos. Sci.* **40**, 1740–1755 (1983).
22. Materials and methods are available as supplementary materials.
23. G. H. Bryan, J. M. Fritsch, *Mon. Weather Rev.* **130**, 2917–2928 (2002).
24. J. D. Doyle, D. R. Durran, *J. Atmos. Sci.* **59**, 186–201 (2002).
25. T. P. Lane, R. D. Sharman, T. L. Clark, H.-M. Hsu, *J. Atmos. Sci.* **60**, 1297–1321 (2003).
26. R. F. Hertenstein, J. P. Kuettner, Rotor types associated with steep lee topography: Influence of the wind profile. *Tellus Ser. A.* **57**, 117–135 (2005).
27. G. M. Heymsfield, R. H. Blackmer Jr.., *Mon. Weather Rev.* **116**, 2200–2224 (1988).
28. G. M. Heymsfield, L. Tian, L. Li, M. McLinden, J. I. Cervantes, *J. Appl. Meteorol. Climatol.* **52**, 1851–1867 (2013).
29. M. P. Jensen *et al.*, *Bull. Am. Meteorol. Soc.* **97**, 1667–1686 (2016).
30. R. B. Smith, *J. Atmos. Sci.* **42**, 2597–2603 (1985).
31. D. R. Durran, *J. Atmos. Sci.* **43**, 2527–2543 (1986).
32. R. B. Smith, *J. Atmos. Sci.* **44**, 269–297 (1987).
33. D. R. Durran, J. B. Klemp, *J. Atmos. Sci.* **44**, 3402–3412 (1987).
34. D. R. Durran, in *Mountain Waves and Downslope Winds* (American Meteorological Society (1990), pp. 59–81.
35. T. L. Clark, W. R. Peltier, *J. Atmos. Sci.* **34**, 1715–1730 (1977).
36. M. E O'Neill, L. Orf, G. M. Heymsfield, K. Halbert, *Zenodo* (2021); https://doi.org/10.5281/zenodo.4584086.
37. L. Orf, Numerical Simulation of Supercell Thunderstorms (at 50 meter resolution) Associated with Above Anvil Cirrus Plumes, *Dryad* (2021); https://doi.org/10.5061/dryad.xsj3tx9fw.

ACKNOWLEDGMENTS

We are grateful to D. Durran and C. Homeyer for helpful discussions and to the developers of the xarray and plotly python software packages. We also thank three anonymous reviewers for their helpful reviews. **Funding:** L.O. was supported in part by NSF grants AGS-1832327 and OAC-1663954. L.O.'s access to the NSF-sponsored Frontera supercomputer was provided by the Texas Advanced Computing Center via grant ATM20006. G.M.H. was funded by the NASA Precipitation Measurement Mission (PMM) and Ground Validation program. **Author contributions:** M.E.O. and L.O. designed the numerical experiments. L.O. ran, processed, and visualized the simulations, and K.H. computed the Lagrangian parcels. G.M.H. provided the MC3E radar measurements and data analysis. M.E.O. conducted the analyses and wrote the paper, and all coauthors assisted in reviewing and editing. **Competing interests:** The authors declare no competing interests. **Data and materials availability:** CM1 is publicly available (www2.mmm.ucar.edu/people/bryan/cm1/). Modifications to source code and routines to run model are publicly available (https://github.com/leighorf/cm1r19.8-LOFS and https://github.com/leighorf/LOFS-read). Simulation input files are included in supplementary materials. Plotting codes (*36*) and 203 GB of model output and trajectory data (*37*) are publicly available. HIWRAP radar data are available at the Global Hydrology Resource Center – Distributed Active Archive Center (https://ghrc.nsstc.nasa.gov/home/field-campaigns/mc3e).

SUPPLEMENTARY MATERIALS

https://science.org/doi/10.1126/science.abh3857
Materials and Methods
Figs. S1 to S9
Data S1 and S2
References (*38*–*43*)

4 March 2021; accepted 10 August 2021
10.1126/science.abh3857

Hydraulic jump dynamics above supercell thunderstorms

Morgan E ONeill, Leigh Orf, Gerald M. Heymsfield, and Kelton Halbert

Science, **373** (6560), .
DOI: 10.1126/science.abh3857

Water up

Above-anvil cirrus plumes are stratospheric cloud formations that form downwind from the tops of some very strong thunderstorms. Despite their common occurrence, an adequate physical model explaining many of their features and effects does not exist. O'Neill *et al*. show that the storm supercell that extends into the stratosphere functions like a physical barrier, deflecting wind streams there like a topographic obstacle and driving a hydraulic jump downstream at the tropopause (see the Perspective by Smith). This feature triggers the intense injection of water vapor deep into the stratosphere, leading to a substantial increase in stratospheric humidity. —HJS